SERI/PR-8278-1-T2

VACUUM DEPOSITED POLYCRYSTALLINE SILICON FILMS FOR SOLAR CELL APPLICATIONS

Second Quarterly Technical Progress Report, January 1—March 31, 1980

By
Charles Feldman
Charles H. Arrington, III
Norman A. Blum
Frank G. Satkiewicz

May 1980

Work Performed Under Contract No. AC02-77CH00178

The Johns Hopkins University
Applied Physics Laboratory
Laurel, Maryland

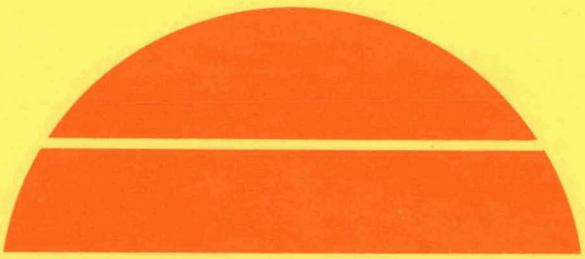

U.S. Department of Energy

Solar Energy

DISCLAIMER

DISCLAIMER

Available from the National Technical Information Service, U. S. Department of Commerce, Springfield, Virginia 22161.

Price: Paper Copy $7.00
Microfiche $3.50

SERI/PR-8278-1-T2
Distribution Category UC-63c

VACUUM DEPOSITED POLYCRYSTALLINE SILICON FILMS FOR SOLAR CELL APPLICATIONS

SECOND QUARTERLY TECHNICAL PROGRESS REPORT

JAN. 1 - MARCH 31, 1980

Charles Feldman, Charles H. Arrington, III,
Norman A. Blum, and Frank G. Satkiewicz

MAY 1980

THE JOHNS HOPKINS UNIVERSITY
APPLIED PHYSICS LABORATORY
LAUREL, MARYLAND 20810

PREPARED FOR THE SOLAR ENERGY RESEARCH INSTITUTE
PHOTOVOLTAIC PROGRAM OFFICE
UNDER SUBCONTRACT XS-9-8278-1

This Second Quarterly Technical Progress Report covers the period Jan. 1 - March 31, 1980, and describes work performed by the Johns Hopkins University, Applied Physics Laboratory for the Solar Energy Research Institute under Subcontract No. XS-9-8278-1. The Subcontract with SERI continues work previously supported for one year by DOE under Interagency Agreement No. ET-78-A-03-2208. C. Feldman is the Principal Investigator. Other professional staff members participating in this investigation are C. H. Arrington, III, N. A. Blum, H. K. Charles, Jr., and F. G. Satkiewicz. Technical assistance was provided by R. B. Givens, K. G. Hoggarth, E. W. Koldewey, and R. Neuwiller.

DESCRIPTION OF PROJECT

This study addresses the goal of fabricating low-cost, 10% efficient solar cells through the use of vacuum deposited, thin film, polycrystalline silicon. Work areas include methods of growing large grains, exploration and optimization of suitable substrate/bottom electrode material, improvement in photovoltaic efficiency, formation of n-layer by vacuum deposition rather than by diffusion, and analysis of film and junction properties. Emphasis is placed at each stage of the program on understanding and elucidating the pertinent physical and electrical phenomena through the judicious use of analytical tools such as secondary-ion mass spectrometry for impurity and compositional analysis and x-ray diffractometry and scanning electron microscopy for structure analysis.

ABSTRACT

A careful study of a specially formed thin silicon layer on TiB_2-coated sapphire reveals that the interaction layer of $TiSi_2$ is composed of larger grains. Processing steps were developed which lead closer to the goal of fabricating polycrystalline silicon photovoltaic devices completely by vacuum deposition. Both n-type and p-type silicon are now being deposited. New deposition masks were made for depositing the n-regions upon the p-layers. New electrode deposition masks were also made for a direct electroding process to replace the photolithographic process used previously. The TiB_2 bottom electrode fabrication has been achieved in a single vacuum chamber. Reaction constants and activation energy for TiB_2 layer formation were determined to be less than those reported by other authors for bulk material. Studies of crystallite growth and interfacial interactions have continued. Major sources of undesirable impurities have been identified and removed from the vacuum chambers. The changes made this quarter have not been incorporated into a completed photovoltaic device.

TABLE OF CONTENTS

LIST OF TABLES

LIST OF FIGURES

1. INTRODUCTION

This is the Second Quarterly Technical Progress Report describing investigations on thin-film polycrystalline silicon solar cells performed under the Solar Energy Research Institute (SERI) Sub-Contract XS-9-8278-1. The work is a continuation of research performed under Interagency Agreement ET-78-A-03-2208 with the Department of Energy.

The study addresses the DOE goal of fabricating low-cost, 10% efficient solar cells through the use of vacuum deposited, thin-film polycrystalline silicon. It is visualized that each step of the solar cell fabrication would be performed in a vacuum chamber and that the complete process would be carried out automatically in a mass production. Investigations being carried out at present correspond to the separate fabrication steps in the formation of all-vacuum deposited solar cells. The cells are formed by successive depositions onto substrates of bottom electrodes, silicon layers, and top electrodes. Since the behavior of each successive layer depends upon what lies below, the entire film system is being examined concurrently.

During this quarter, steps were carried out which further lead toward the goal of completely fabricating the photovoltaic devices by vacuum deposition. The oil-diffusion-pumped vacuum system, formerly used to produce the p-type layers, was converted to fabricate the n-type layer; the ion-pumped system, formerly used for crystallite studies, was converted to p-type deposition. Work was begun on the formation of n-type silicon films through the deposition of silicon in a controlled phosphine atmosphere. Polycrystalline n-doped films were formed and are being evaluated (Section 2.3). Evaporation masks were used in the formation of top metal electrodes to replace the photolithographic process described in prior reports. Unfortunately, the original set of masks for the electrodes proved unsatisfactory and a new set of masks had to be fabricated (Section 4.1).

The TiB_2 bottom electrode fabrication took place in a single vacuum chamber instead of depositing the Ti and B in separate chambers (Section 3.1). A 12-substrate holder to increase production capability was used in the formation of the bottom electrodes. This will aid in supplying electroded substrates for both the n-type and the p-type silicon depositions. Studies on the reaction between Ti and B in the formation of TiB_2 layers were conducted in order to determine the process reaction rates.

Studies of the deposition of p-type silicon were continued. A run was made in which the island or initial cluster formation could be observed throughout the entire sample. In previous studies the cluster formation was observed only on the edges of wedge-shaped samples and a question remained whether the same behavior occured during the normal deposition procedure (section 2.2). Efforts were made to improve the purity of the silicon films in the ion-pumped system. The Mo, Cr, Ti and Al impurity levels were reduced by about an order of magnitude (Section 2.1).

Because of changes in operating techniques as a prelude to an all vacuum-produced cell and because of the requirements for new masks, only three photovoltaic devices were completed this quarter (Section 4).

2. SILICON FILM FORMATION

2.1 p-Type Silicon Films

Both n-type and p-type silicon layers were formed during this reporting period. The n-type films were formed in the oil-diffusion-pumped system and are described in Section 2.3.

The p-type silicon films formed this quarter are listed in Table I.

TABLE I

SILICON FILM PARAMETERS

Sample	Substrate	Sub. Temp. (°C)	Thickness (μm)	Deposit Rate Å/min	Remarks
Si*240A	Alumina				
B	Sapphire/$TiB_2$276E	1220			(G) Boron $2 \times 10^{17}/cm^3$
C	Alumina/$TiB_2$276A				
D	Alumina				
E	Alumina/$TiB_2$276B				
F	Alumina				
G†	Sapphire		12	400	
Si*241A	Alumina				
B	Alumina/$TiB_2$280B	1265			Thin non-continuous on (B), (C), & (E).
C	Sapphire/$TiB_2$291C				
D	Alumina				
E	Sapphire/$TiB_2$287A				
F	Alumina				
G†	Sapphire		5	420	
Si*242A	Alumina				
B	Alumina/$TiB_2$290B	1270			(F) Boron $5.2 \times 10^{17}/cm^3$
C	Alumina				
D	Sapphire/$TiB_2$287B				
E	Alumina/$TiB_2$281C				
F	Sapphire				
G†	Sapphire.		11.5	760	
Si*243A	Alumina				
B	Silicon P .001-.005 Ω/cm	1175			(B) Grew epitaxially
C	Alumina/$TiB_2$290D			60 min≈ 400 then 87 min≈ 900	(F) Boron $7.5 \times 10^{16}/cm^3$
D	Sapphire/$TiB_2$290C				
E	Alumina/$TiB_2$291F				
F	Sapphire				
G†	Sapphire		10		
Si*244A	Alumina				
B	Sapphire/$TiB_2$297A	1240			(F) Boron $3.4 \times 10^{16}/cm^3$
C	Sapphire/$TiB_2$297F			60 min≈ 400 then 150 min≈ 900	
D	Alumina				
E	Alumina/$TiB_2$297E				
F	Sapphire				
G†	Sapphire		14.8		

† The "G" sample is located outside the heated area to enable thickness measurements on a non-grainy layer.

The samples were deposited by electron beam deposition at a beginning pressure in the mid 10^{-8} Torr range, and a final pressure in the mid 10^{-9} Torr range. This pressure is two orders of magnitude lower than was obtained in the oil-pumped system. Base pressure in the system, in the absence of heat or deposition, is in the 10^{-10} Torr range. The water vapor pressure in the system is still higher than desired and a cryogenic pump is on order to further reduce this pressure.

Samples Si*243 and Si*244 were deposited using the normal electron beam power of 1.5 kw for approximately one hour, then the power was increased to approximately 2.1 kw in order to achieve a faster rate for the remainder of the deposition. These beam powers correspond to roughly estimated deposition rates of 400 Å/sec and 900 Å/sec, respectively. The rates are not known precisely because previous calibration runs of electron beam power vs rate were carried out in a different system (oil-pumped) using a different high voltage power supply. The object of the dual rates was to allow large seed growth at the slower rate while achieving higher film purity at the faster rate. The results of these runs are inconclusive at present because changes in the vacuum system, described below, were also made.

As discussed in the First Quarterly Report,[1] it is believed that impurities may be limiting the efficiency of the photovoltaic devices. Efforts were carried out to reduce particularly the molybdenum and titanium content of the films. The results of the efforts are shown in Table II. Si*236E represents the typical impurity levels recently observed in the samples deposited in the ion-pumped chamber. These impurity levels were higher than those observed in samples deposited in the oil-pumped system. Si*242F shows the impurity levels after the Ti-Mo alloy filaments in the titanium getter pump were changed to Ti wound tungsten filaments. As can be seen, neither the Ti nor the Mo levels were reduced. In Si*243F and Si*244F further sources of molybdenum were removed.

The Mo wires to the electron-beam gun and heat lamps were replaced with Ta wires. Further, the Mo electrodes of the quartz heat lamps were shielded with Ta sheets. As can be seen in Table II, these changes yielded a significant reduction in the B, Mo, Cr, Ti and Al levels. It is believed that the reaction of Mo with water vapor produces a volatile species which enhanced the Mo contamination. It is possible that the effect of removing the Ti-Mo sublimation filaments did not show up until the 2nd or 3rd deposit. Samples Si*243 and Si*244 were also deposited at the normal rate followed by a faster rate, which may account for the further impurity reduction.

TABLE II

IMPURITIES IN SILICON FILMS

[Concentration, (X 10^{18}) atoms/cm^3 †]

Species	Si*236E	Si*242F	Si*243F	Si*244F
B	0.88	0.52f	0.75	0.034, 0.024f
C		1.7f		3.9f
O		8.8f		16.7f
Al	0.24	2.3f	ND	0.066f
Ti	0.058	0.057, 0.13f	0.03	0.0013, 0.047f
Cr	0.14	0.016, 0.88f		
Mo	0.18	2.4, 1.9f	< 0.04	< 0.02, < 0.05f

† A defocused beam with oxygen enhancement was used for analysis except for values followed by "f" referring to focused beam without oxygen.

ND = Not detected

2.2 Silicon Crystallite Study

2.2.1 Island Formation of Si*241C

In the last quarterly report a study was described in which wedge-shaped samples were formed in order to observe the island or cluster formation which occurs in the initial stages of silicon deposition. It was pointed out in that report that the thin wedges

may not represent the true conditions of deposition because the deposition rate in the shadowed region is very slow compared to the normal deposition rate. Therefore, a sample (Si*241C) on a TiB_2/sapphire substrate was formed just thick enough to observe the island formation but using the rate and temperature of a more or less normal deposition. (See Table I.)

The sample (Si*241C) was carefully examined by SIMS, SEM and x-ray in an effort to understand the grain growth which occurs in the layers. A phenomenon was observed which was somewhat different than expected, knowledge of which may help in the future formation of silicon films. The observation is that the large silicon grain growth does not begin with pure silicon growth out of small grained TiB_2-$TiSi_2$ as previously believed, but rather out of seemingly large crystals. These large crystal areas appear to be mostly $TiSi_2$, but an unknown phase of Ti-Si-B composition may also be present. Observations leading to this tentative conclusion are presented here.

2.2.2 SIMS Analysis of Sample Si*241C

Si*241C showed uniformly distributed islands of crystallites which were identified as Si by SEM (Section 2.1.3). A SIMS analysis was conducted with a defocused beam of 10 keV Ar^+, using both atomic and polyatomic spectra in order to study the phase distribution in the samples. Figures 1 and 2 show the intensity fraction vs time plots of selected atomic and polyatomic ions. The phases that are observed to be present are Si (elemental), $TiSi_2$, TiB_2, and by material conservation, SiB_x. Polyatomic spectra of the pure phases were used to provide a set of relative ion yield factors (Table III) which helps determine to some extent the degree to which phase decoupling is possible. In addition, selected polyatomic ion ratios (such as TiB^+/Ti^+, SiB^+/Si^+, etc.) were used. The delineation of $TiSi_2$ and TiB_2 is fairly straightforward, but

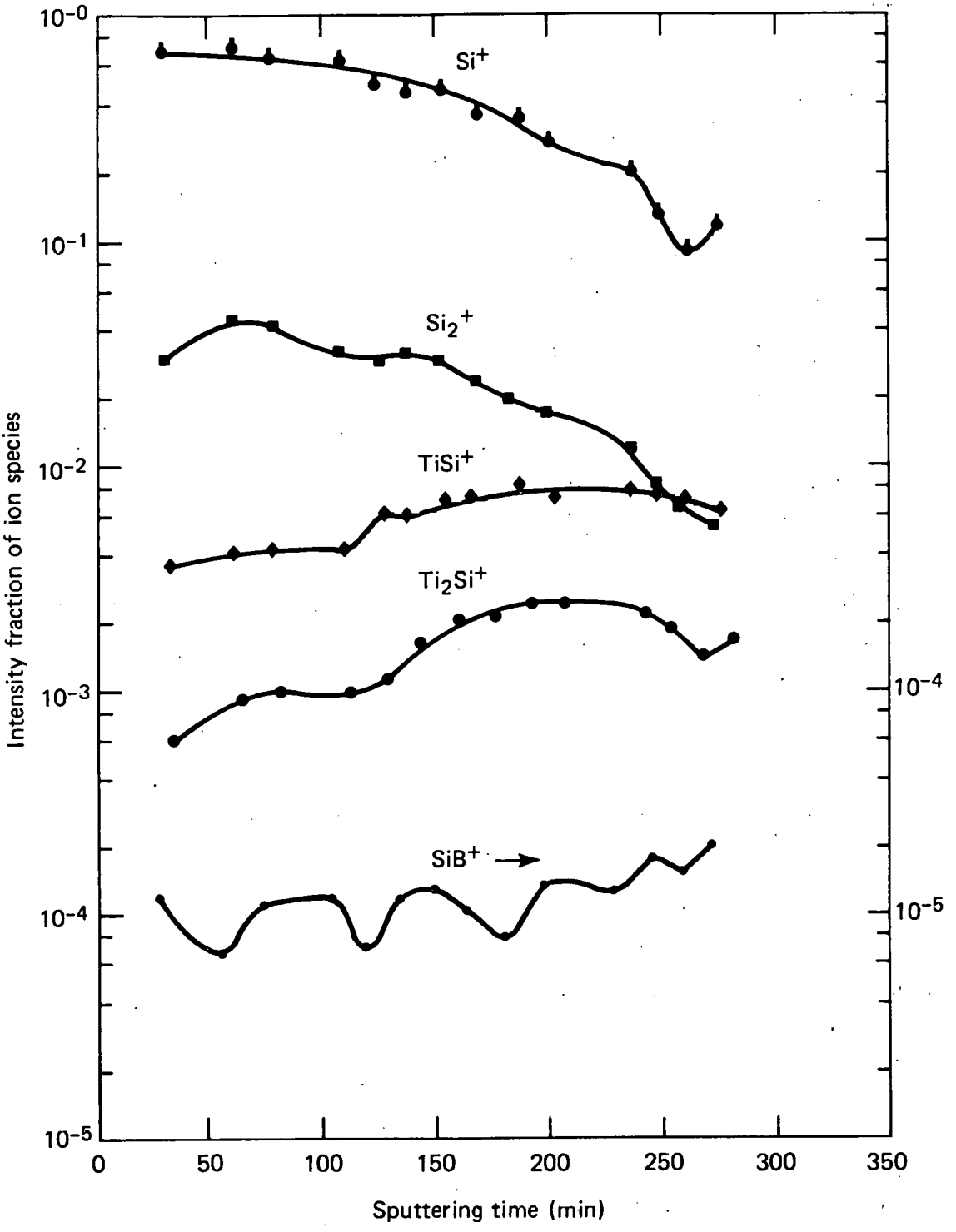

Fig. 1 Intensity-time profiles of ion species from several phases; sample Si*241C.

the detection of SiB_x is hampered by three factors:

1) Small amounts are predicted to be present from the equation

$$7Si + 3TiB_2 \rightarrow 3TiSi_2 + SiB_6 \quad ; \qquad (1)$$

2) Relatively low ion yields exist for both Si^+ and B^+ (as well as polyatomic ions such as SiB^+); and

3) Interference at SiB^+ (39) from K^+ (39) and at SiB^+(38) from AlB^+ (38) for bulk SiB_6 lead to poor calibration values.

A qualitative analysis of the intensity profiles leads to the following observations:

a. The predominant phase on or near the surface (0.38 μm) is silicon with a smaller amount of $TiSi_2$ and a much smaller amount of boron. A semi-quantitative estimate based on the values in Table III and a knowledge of the spectra of the pure phases gives: 0.89 Si, 0.096 $TiSi_2$, 0.014 SiB_6, and 0.0082 TiB_2. This composition, expressed as a phase fraction, is consistent with SEM estimates.

b. A relatively abrupt change in the boron bearing peaks occurs after ∿ 60 min of sputtering corresponding to the removal of about 0.9 μm of material. This is interpreted as having sputtered off regions containing a relatively thin coat of Si.

c. Removal of ∿ 2 μm (∿ 125 min) gives a projection containing $TiSi_2$ (and, by inference, SiB_x) and increasing amounts of TiB_2. Silicon is steadily diminishing. At this point a semiquantitative estimate for the composition is: 0.34 Si, 0.36 $TiSi_2$, 0.19 TiB_2, and 0.12 SiB_6.

d. After the removal of 4 μm (260 min), the Si peaks are reduced substantially and the boron bearing peaks have almost plateau values. The estimated composition is: 0.34 $TiSi_2$, 0.55 TiB_2, and 0.11 SiB_6.

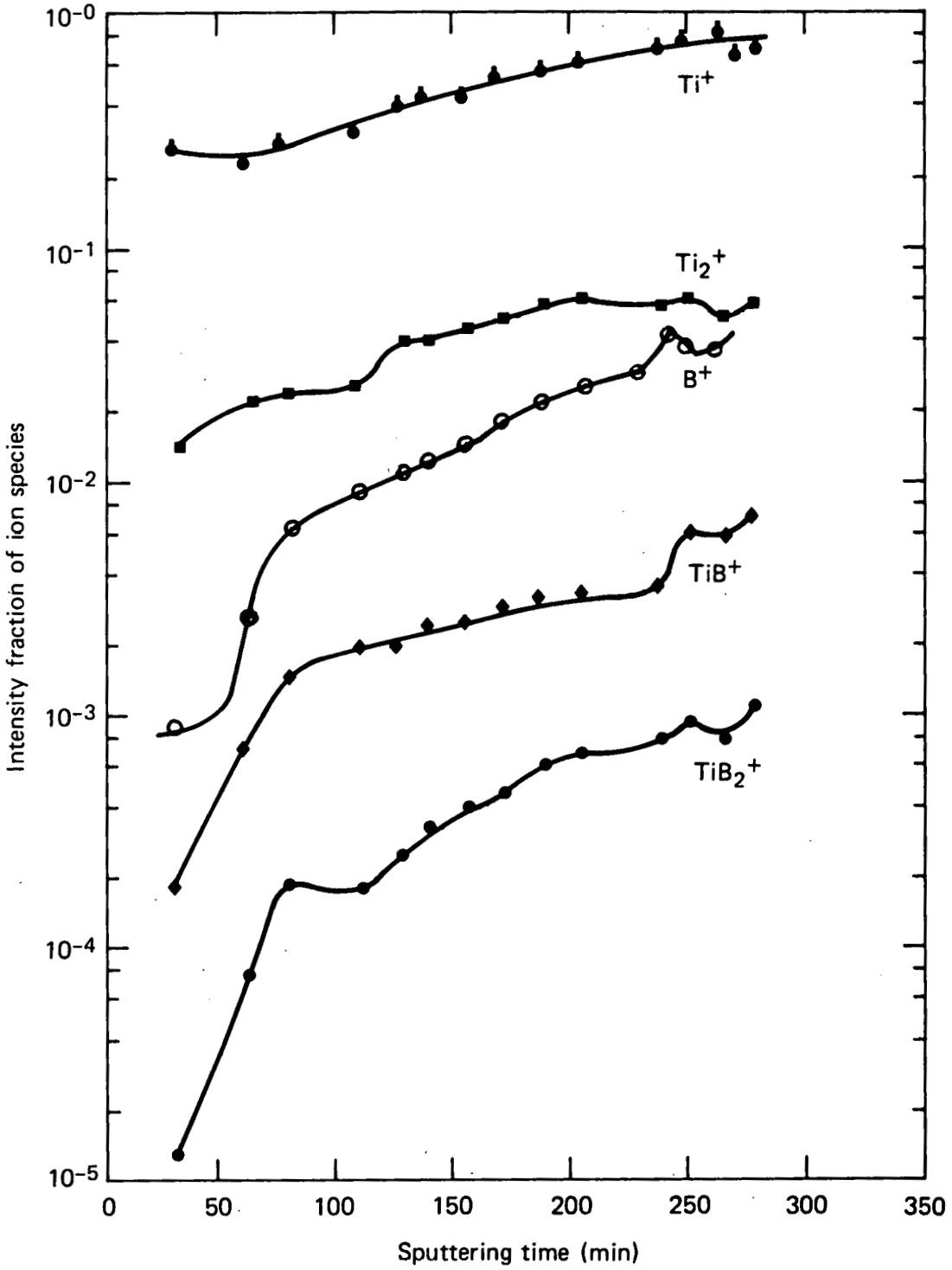

Fig. 2 Intensity-time profiles of ion species from sputtering sample Si*241C.

TABLE III

RELATIVE ION YIELDS IN A POLYPHASE SYSTEM*

Species	Y ($Y_{Ti,\ TiB_2} = 1$)
Ti (TiB_2)	1.0
Ti ($TiSi_2$)	2.0
B (TiB_2)	0.074
B (SiB_6)	0.061
Si ($TiSi_2$)	0.28
Si (SiB_6)	0.093
Si (e)	0.41

* Major isotope; energy window of 250 ± 25 eV.

2.2.3. Scanning Electron Microscope Examination of Si*241C

An electron microscope image of the surface of sample Si*241C is shown in Figure 3. The large silicon crystallites are in the form of islands distributed throughout the surface of the sample. Three different size crystallites are observable: 1) large silicon crystals; 2) smaller crystallites identified as $TiSi_2$; and 3) very small crystallites identified as TiB_2 that are observed in limited regions (holes) in the $TiSi_2$ structure. Identification of these three regions was carried out using the x-ray emission microprobe capability of the SEM (boron cannot be identified by this technique). Figure 4 shows the x-ray emission spectrum of regions A & B, as labeled in Figure 3. Identification was aided by both SIMS and x-ray microprobe.

Following the SIMS analysis, the bottom of the crater formed by sputtering was examined by SEM. Figures 5a and 5b present the photomicrographs of the bottom of the crater and of an adjacent region on the sample surface; both images are at the same magnification. The regions in Figure 5b were again examined by microprobe;

the only pure silicon remaining was in areas having the appearance of region B and showed up as small peaks growing from the larger flat regions labeled A. These larger, flat, apparently single-crystal regions were identified by the microprobe as containing Ti and Si. SIMS analysis indicated that boron is also present. The large crystallites thus appear to be a composition of $TiSi_2$ plus a phase containing boron.

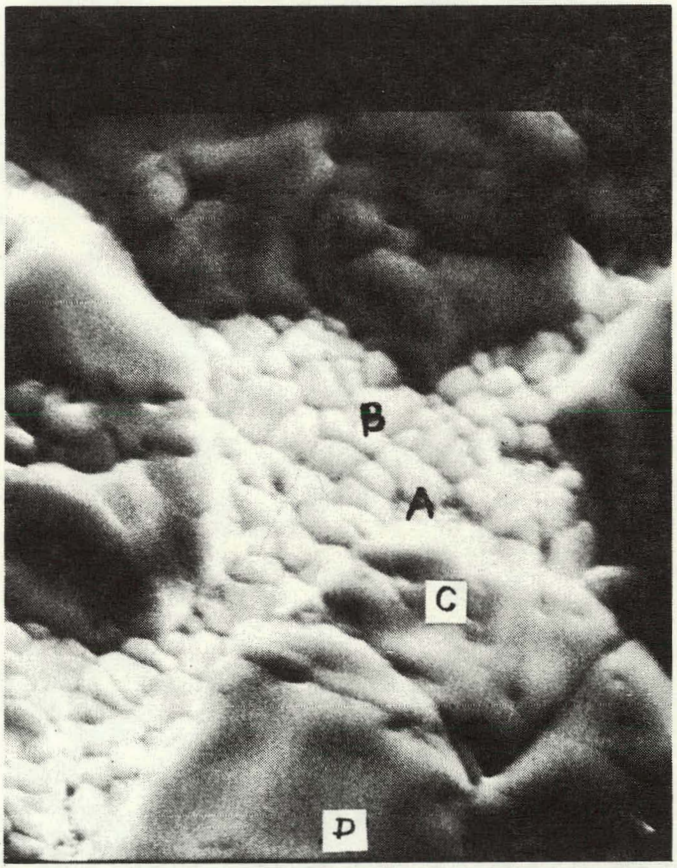

Fig. 3 SEM photomicrograph of 5 μm silicon film illustrating cluster-formed regions. Region A - TiB_2, Region B - $TiSi_2$, Region C & D - silicon.

(a)

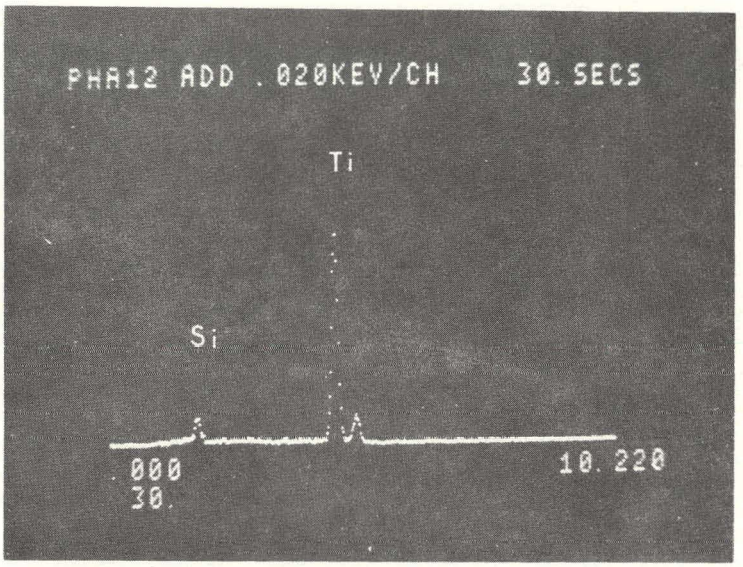

(b)

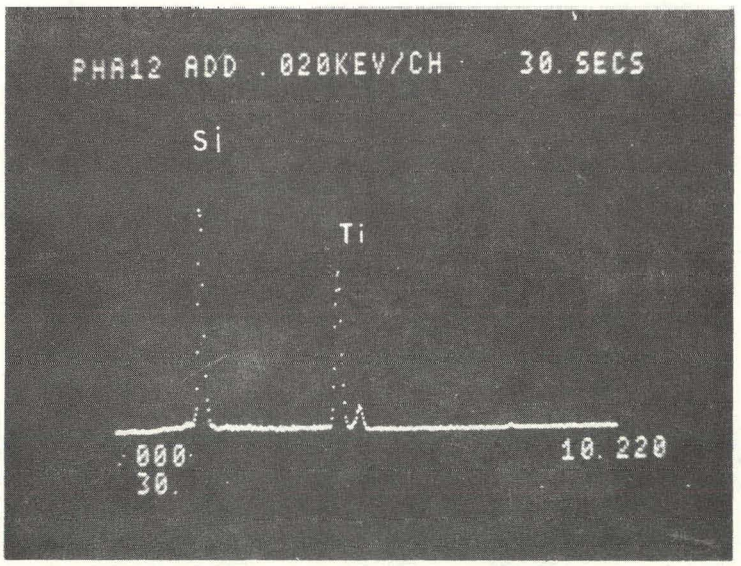

Fig. 4 SEM microprobe x-ray spectrum of regions in Sample Si*241C
a. Region A b. Region B

(a) outside

(b) inside

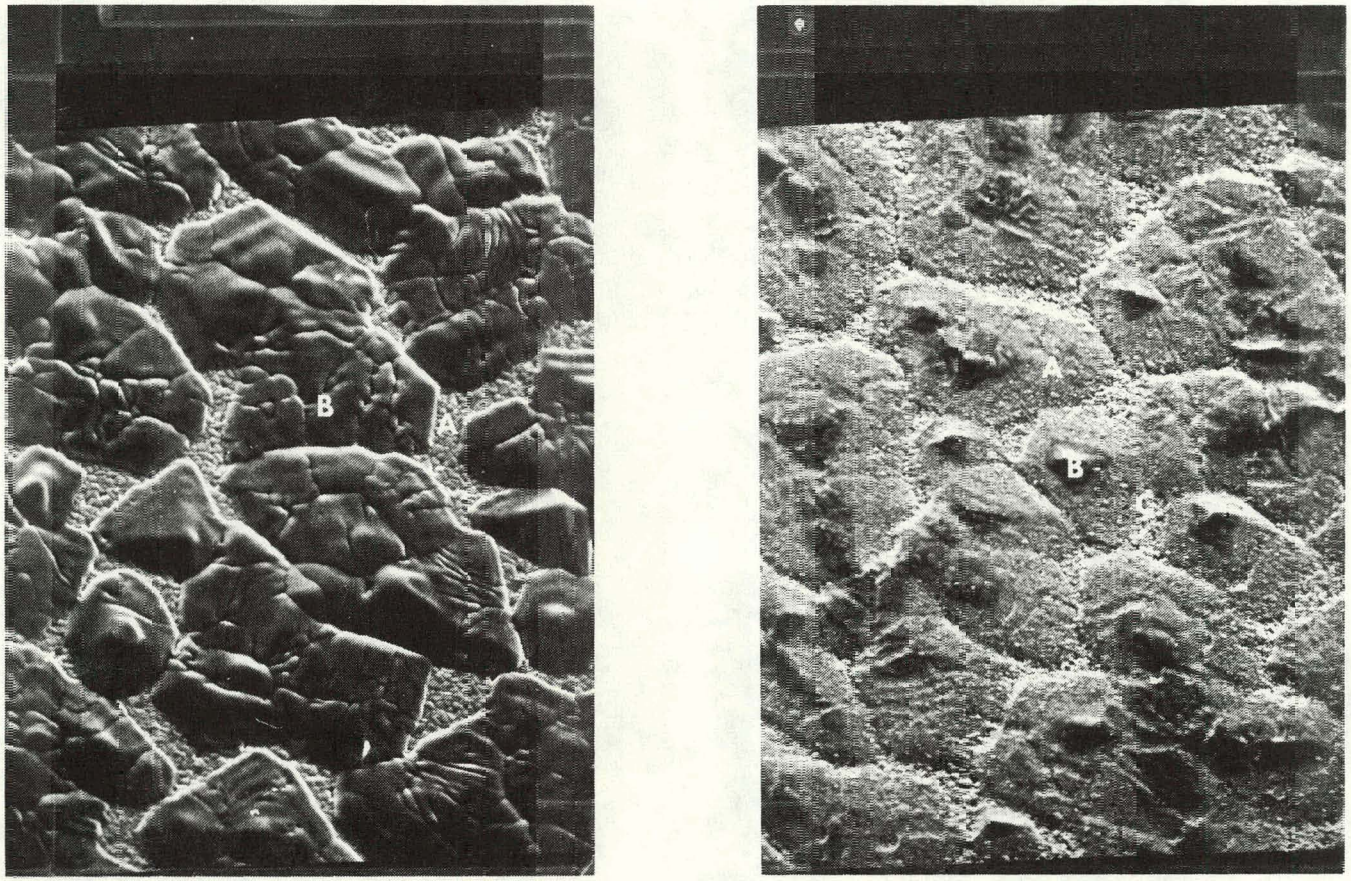

Fig. 5 SEM photomicrograph of Si*241C (440X) of region inside and outside sputtered crater.

A - $TiSi_2$

B - silicon

C - titanium, silicon, aluminum and boron

2.2.4 X-ray Analysis of Si/TiB_2/Sapphire

An x-ray diffraction analysis of sample $Si*241C/TiB_2 287A$ on a sapphire substrate was carried out using the Seifert 180-1000 x-ray generator, Cu target x-ray source, and Read thin film camera, all of which were described in earlier Quarterly Progress Reports.

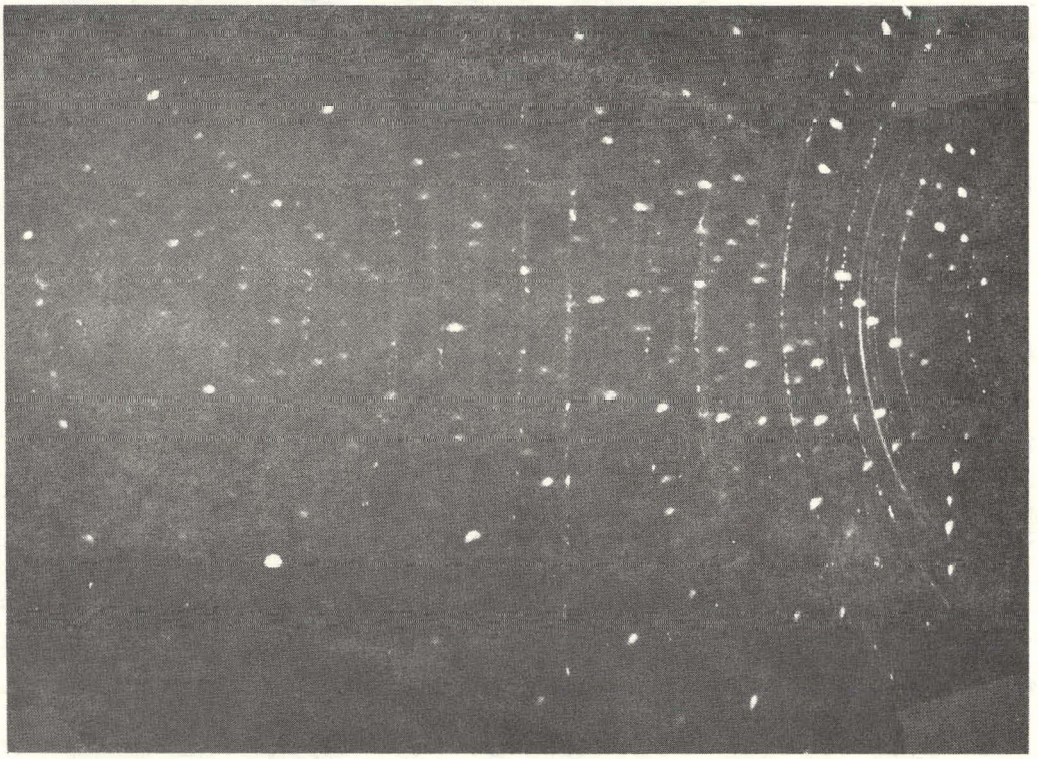

Fig. 6 X-ray diffraction pattern from Read thin film camera; sample Si*241C.

A photograph of the x-ray diffraction pattern is shown in Figure 6. The intense spots are due to the sapphire substrate; the continuous arcs (lines) arise from the various polycrystalline phases present in the layers of the deposited film. The d-values (lattice spacings in units of 10^{-10} m) associated with each of the arcs was obtained from a visual reading of the line positions using a manual, micrometric, cross-wire illuminator. Table IV lists all of the observed lines, their visual characteristics and the Powder Diffraction File (PDF) line positions for Si, TiB_2, $TiSi_2$ and SiB_6.

The line positions are given to three significant figures, even when more accurate values are available in the PDF. The line characteristics (column 2 of Table IV) represent visual judgments. The number after the slash in column 3 indicates the approximate relative line intensity (100 - strongest line). The camera and readout method permit approximately three significant figure accuracy in the d-values (e.g., 1.38 $\pm$ .01), and lines within .02 units of each other are generally not resolvable (the resolution is actually a weak function of the d-value).

The grainy lines indicate the presence of (relatively) large crystallites. These lines in Si*241C are identified exclusively with Si and $TiSi_2$, indicating that these phases are composed of large crystallites. The crystallite size can be inferred, in principle, from the graininess of the diffraction lines; however, we have not done this quantitatively. The smooth lines were identified with the fine grained phase, TiB_2. The relatively large grain size of Si and $TiSi_2$ compared with TiB_2 is verified by the SEM studies (Sect. 2.2.3). All lines of Si, TiB_2, and $TiSi_2$ are accounted for, although some are not uniquely represented because of limited camera resolution.

In order to explain the presence of expected boron from the reaction of TiB_2 with silicon (Eq. 1, Sect. 2.2.2), other possible phases containing Si, Ti and possibly Al (from the substrate) with B were sought. The only phase listed in the PDF which comes close to agreeing with the observed x-ray pattern is SiB_6, the d-values of which are listed in the last colume of Table IV. For several reasons, however, the conclusion is that SiB_6 is probably not a significant constituent of the sample: (a) the strong line at 2.93 is outside the $\pm$ .01 experimental limit of error, (b) all five of the other strong lines overlap identified lines of one or more of the identified phases, and most significantly, (c) strong lines of SiB_6 at 2.40 and 0.81 are not seen at all. Another possible constituent is SiB_{14} which has its strongest lines for $d \geq 4.100$. The present experimental arrangement does not permit observation of lines with $d \geq 3.50$, so that confirmation or rejection of the presence of SiB_{14} cannot be certain at this time.

TABLE IV

X-RAY DIFFRACTION LINES FROM Si*241C (ON SAPPHIRE)

d	Char.	Si	TiB_2	$TiSi_2$	SiB_6
3.22	W		3.22/20		
3.13	SG	3.14/100			
2.96	VVW				
2.91	VWG				2.93/100
2.63	W		2.62/60		
2.30	SG			2.29/100	
2.14	MG			2.13/70	
2.09	MG			2.08/90	2.07/70
2.03	S		2.03/100		
1.99	VVW				
1.92	SG	1.92/60			
1.89	VW				
1.83	MG			1.82/90	1.85/90
1.78	VWG				
1.64	SG	1.64/35			
1.62	W		1.61/14		
1.53	VVWG			1.54/20	
1.52	VVWG		1.51/20	1.49/20	
1.38	VVW			1.39/70	1.38/90
1.37	M		1.37/26		
1.36	MG	1.36/8		1.36/70	
1.32	WG		1.31/8	1.31/90	1.31/90
1.25	MG	1.25/13		1.24/70	
1.22	VW		1.22/14	1.22/60	
1.20	VVW			1.19/90	
1.11	MG	1.11/17	1.10/12	1.08/60	
1.05	MG	1.05/9		1.07/60	
1.02	VVW		1.02/12		
0.998	W		0.996/9		
0.958	VVWG	0.960/5			
0.950	W		0.948/10		
0.918	MG	0.918/11			
0.861	WG	0.859/9			
0.846	W		0.845/6		0.85/90
0.833	VW		0.832/6		
0.829	VVWG	0.828/5			
		Missing lines > 10% relative intensity			
		none	none	none	2.40/90 0.81/90

M-Medium, W-weak, S-Strong, V-very, G-grainy

There are five tentatively unidentified (out of 36) lines in the diffraction pattern, including the one at 2.91, possibly associated with SiB_6 or SiB_{14}. All are classed as very, or very very weak. There are a number of reasons for the observation of weak unidentified lines: (a) presence of an unidentified phase, (b) lines of an identified phase not listed in PDF, (c) impurity phases in a small fraction of an identified phase. Other x-ray diffraction analyses of different samples usually also exhibit a few unidentified lines, but (with one possible exception) the unidentified lines are frequently different from sample to sample. It has been, so far, impossible to identify with certainty any additional phases being formed in the samples which show up in the x-ray diffraction patterns.

2.3 n-Type Silicon Formation

The oil-diffusion-pumped vacuum system was adapted to form n-type silicon layers by deposition of silicon in a phosphine (PH_3) atmosphere. This system was selected for the n-type deposit because it has a mechanical backing pump which is vented to the outside, making it safe to use with poisonous gas.

The system was fitted with a phosphine gas line which enters the deposition chamber through a leak valve, thus allowing the silicon deposition to take place in an accurately controlled partial pressure of phosphine. At elevated substrate temperatures some of the phosphine molecules striking the substrate dissociate. With no silicon being deposited, most of the phosphorus and its hydrogen compounds re-evaporate from the substrate surface; but during deposition of the silicon a certain fraction of the phosphorus is trapped in the deposit. The segration coefficient for phosphorus in silicon is large, ensuring the doping of the silicon. In keeping with the usual system of sample designation, the n-type silicon samples will be listed sequentially as N-Si _____.

An initial run, at a substrate temperature of 950°C, was made and n-type polycrystalline silicon films (n-Si 1) 1 μm thick were successfully deposited onto sapphire, ceramic, and crystal silicon substrates, and also onto previously-deposited p-type silicon thin films. The conductivity type was checked with a thermo-electric probe. The concentration of phosphorus depends mainly on the phosphine partial pressure and the silicon deposition rate. For a partial pressure of 2×10^{-6} Torr and a deposition rate of 160 Å/min, the electrically active phosphorus concentration was determined to be 2×10^{17} atoms/cm^3 from resistivity measurements ($\rho = 0.06$ Ω-cm); this corresponds to about one electrically active phosphorus atom being trapped for every 10^5 that are incident on the substrate. SIMS measurements give about 3×10^{19} atoms/cm^3 for the total phosphorus concentration.

In order to form a junction between a deposited n-layer and a p-type substrate, it is necessary to remove the oxide layer from the p-type silicon. This can be done by depositing silicon at about 1100°C, at which temperature the silicon will react with the silicon dioxide to form volatile silicon monoxide. A film 2 μm thick was deposited at this temperature, again at 2×10^{-6} Torr partial pressure of phosphine. The resistivity of these films increased to 6 Ω-cm, apparently due to the shortened dwell time (due to the higher temperature) of the phosphorus atoms on the silicon surface. In addition, silicon surfaces that were exposed to the gas, but which received no deposit, became n-type due to diffusion of the gas into the surface.

To eliminate these problems, the final run in this reporting period consisted of an initial, short deposit of silicon (∿ 20 Å) at 1100°C, followed by a long run in a 2×10^{-6} Torr phosphine atmosphere at 950°C. The resulting film, 0.4 μm thick, again had a resistivity of about 0.1 Ω-cm, as in the initial run. Faster evaporation rates to increase the phosphorus concentration through trapping will be tried and n^+-p junctions will be formed and studied in the next reporting period.

3. THE BOTTOM ELECTRODE

3.1 TiB_2 Formation

Work continued this quarter on the deposition of TiB_2 films needed in both the formation of photovoltaic devices and in the study of the kinetics of TiB_2 formation. These two aspects of the research required different types of samples. The samples used for the formation of photovoltaic devices are thick, (generally about 1 μm) and are heated longer than required for the complete TiB_2 reaction. Sufficient time should be allowed for the removal of excess boron by a water vapor or oxygen reaction on the surface. The samples used in exploring the kinetics of the Ti-B reaction are thin samples amenable to examination by SIMS without loss of resolution and are reacted only partially so that the kinetics of the reaction may be observed (Table VI). The result of the SIMS investigation, as described in the next section, indicates that the reaction constants of the thin film Ti/B couples produced here are considerably less than those reported for the bulk material.

The TiB_2 sample parameters discussed in this report are listed in Table V. The average resistivities for each run are listed in order to avoid a lengthy table. The resistivities on the sapphire are generally lower than on the alumina substrates. It is believed that this is due either to the surface roughness of the alumina substrate or to a loss of Ti due to a reaction between Ti and sapphire. Sample $TiB_2$297 represents the first run carried out by depositing titanium and boron in the same vacuum chamber without breaking the vacuum. Previous to this run the titanium deposit was made in a separate, small, 10"-pyrex chamber and its thickness was measured prior to placing it in the 12"-stainless-steel chamber where the boron deposition was carried out. In order to produce samples without breaking the vacuum, a number of runs were made in order to establish the deposition rates of the titanium and boron depositions. The depositions were carried out in the 12"-stainless-steel, commercial vacuum system with the source-to-substrate distance approximately

19.5 centimeters. Titanium was deposited from a tungsten boat at a rate of approximately 0.1 μm/min. The tungsten boat was changed after each deposition to avoid excess alloying of titanium and tungsten. Tungsten desolves in the titanium melt, raising the melting point and making it difficult to control accurately the deposition rate after the first run. The boron was deposited by electron-beam heating of pure boron in the molybdenum-lined, water-cooled crucible. The deposition rate was approximately 0.08 μm/min. At this stage in the process the chamber was opened; each sample is measured and then replaced in the chamber for reaction. This measurement step is necessary in order fully to understand the formation process. While the average resistivities of samples deposited without breaking the vacuum may be somewhat lower than previous samples, further runs are required to confirm this.

TABLE V

TiB_2 Film Parameters

Sample	Ti Thickness μm	B Thickness μm	TiB_2 Calculated Thickness μm	Calculated Excess μm	Formation Temp °C	Formation Time hr	Average Resistivity μΩ-cm
Two chambers							
$TiB_2$276	1.35	0.81	1.37	0.41 Ti	950	3	ND
$TiB_2$280	0.29	0.30	0.42	0.66 B	950	4	∿ 300
$TiB_2$281	0.53	1.12	0.77	0.12 B	950	16	94
$TiB_2$287	0.30	0.50	0.42	0.24 B	950	3	78
$TiB_2$290B	0.83	0.75	1.20	0.44 B	950	5	159
290 C,D	"	"	"	"	"	8	128
$TiB_2$291C	1.29	1.18	1.87	0.77 B	950	3.5	73
291F	"	"	"	"	"	5.5	103
One chamber							
$TiB_2$297	0.81	0.78	1.18	0.08 B	950	3	61
$TiB_2$298	0.65	0.94	0.95	0.39 B	950	3	61
$TiB_2$299	1.29	1.13	1.88	0.08 B	950	3	79
$TiB_2$300	0.68	1.12	0.99	0.53 B	950	3	85

The resistivities, however, are not as low as previously reported for thinner samples or for bulk values and, as indicated in the next section, some of the thick samples were not heated sufficiently. During the next quarter it is planned to react the samples, without breaking the vacuum, for times consistent with the newly determined rate constant.

In order to produce sufficient TiB_2 samples required to supply both the n and p-type silicon film research, beginning with $TiB_2$300 a new substrate holder which contains twelve samples in place of the usual six is being employed. The twelve-substrate holder was initially made of stainless-steel but is being replaced by tantalum in order to avoid contamination of the samples during the high temperature firing stage.

3.2 SIMS Study of Titanium Diboride Film Formation

The proper and efficient formation of the titanium diboride bottom electrode (Al_2O_3 substrate) requires a knowledge of the rate constant for the reaction:

$$Ti\ (s) + 2B\ (s) \rightarrow TiB_2\ (s) \qquad (p,T) \qquad (2)$$

This interaction was studied by Thebault et al.[2] and was conducted using relatively thick fiber and flat samples. Thebault's samples were heated for up to hundreds of hours and resulted in reacted zones in the tens of μm thick. It was of interest to see if the kinetics are the same for the substantially thinner samples used in our work. To study this, several thin Ti-B samples were deposited on sapphire to provide optimum depth resolution conditions for the SIMS analysis. The thicknesses of the two layers were obtained for each sample chosen for study using an optical interferometric technique. Concentration vs depth profiles of an unreacted couple were obtained and discussed in the First Quarterly Report. A companion sample which had been heated for a relatively

long period (30 min @ 950°C) in terms of Thebault's predicted time for full reaction was also analyzed. The continuation of this work this quarter consisted of heating samples for periods short enough and at temperatures low enough to assure incomplete reaction.

Calculated concentration vs depth profiles are shown in Figures 7 and 8 for two films heated at 750°C for 7 min and 850°C for 7.8 min, respectively. These samples, as well as others related to this SIMS study, were reacted in a fused silicon tube furnace flooded with flowing pure He. The samples were inserted and removed in a time considerably shorter than the reaction time. The diffusion limited reaction leads to a rate constant k given by:

$$k = \frac{x}{\sqrt{t}}, \qquad (3)$$

where x is the thickness of the reacted TiB_2 layer and t is the reaction time. Equation (3) was used to obtain the experimental rate constant for the thin films. The value of x formed in time t was found by graphical integration under the TiB_2 profiles. Thicker deposits (samples $TiB_2$299B and $TiB_2$287D) were also analyzed for obtaining higher temperature points. The profiles for $TiB_2$299B are shown in Figure 9. The sample parameters and calculated rate constants (k) are shown in Table VI.

TABLE VI

TiB_2 SAMPLES USED IN REACTION STUDIES

Sample	Film Thickness Ti A	Film Thickness B A	Reaction Temp. °C	Reaction Time min	Reacted Thickness TiB_2 A	k X 10^{-7} cm $sec^{-\frac{1}{2}}$	Ref(2) k X 10^{-7} cm $sec^{-\frac{1}{2}}$
$TiB_2$285D	1178	1914	750	7	585	2.8	4.2
$TiB_2$285C	1325	1767	850	7.8	1090	5.0	13.5
$TiB_2$299B	12900	11100	950	180	12200	11.7	31.6
$TiB_2$287D	3828	4123	1000	11.0	3640	14.2	46.4
Act. energy, E, k cal/mol						18	25

* Graphical integration of TiB_2 profile

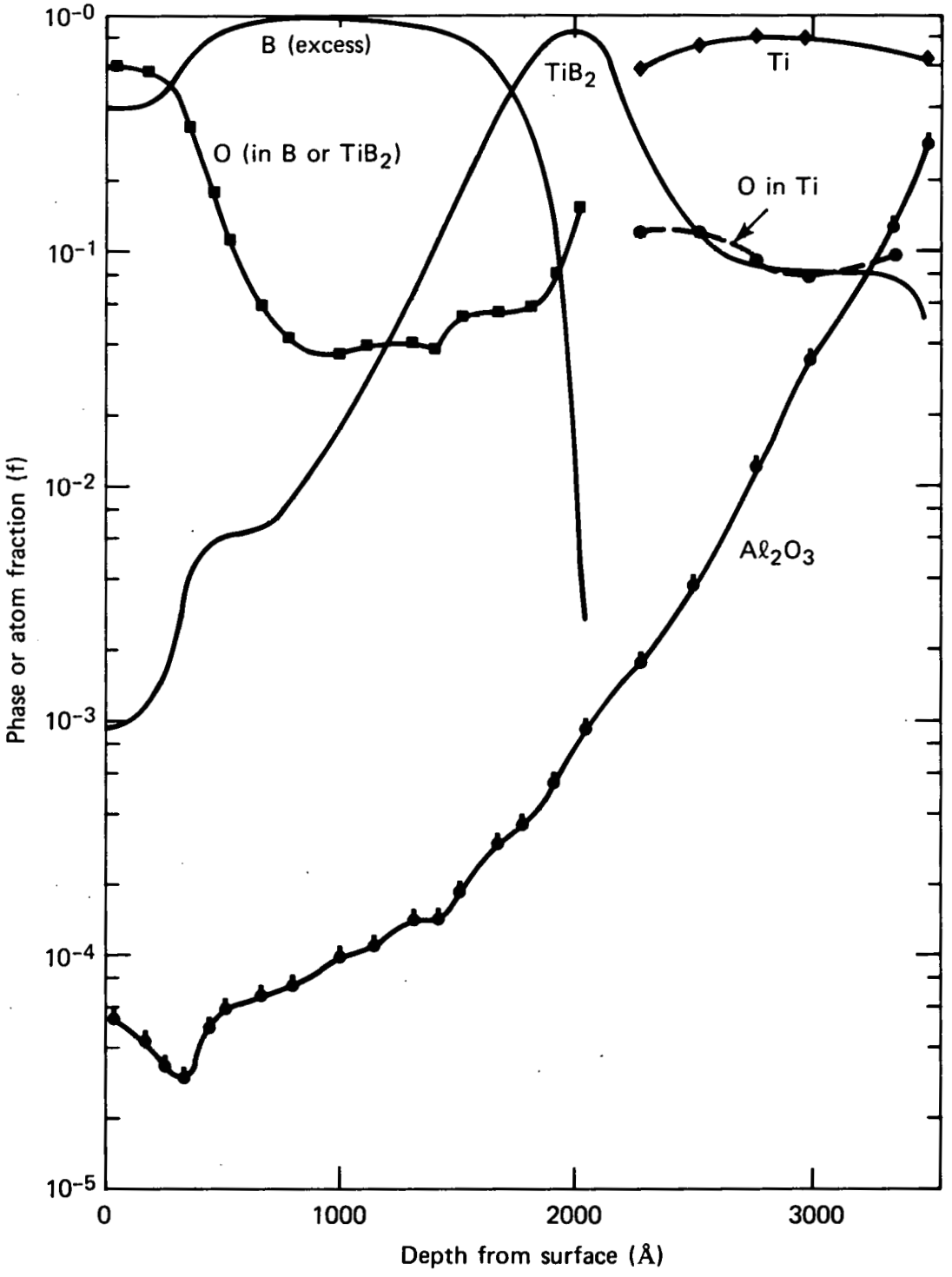

Fig. 7 Concentration-depth profiles from the sputtering of sample $TiB_2$285D (B/Ti/sapphire heated in a He atmosphere for 7 min. at 750°C).

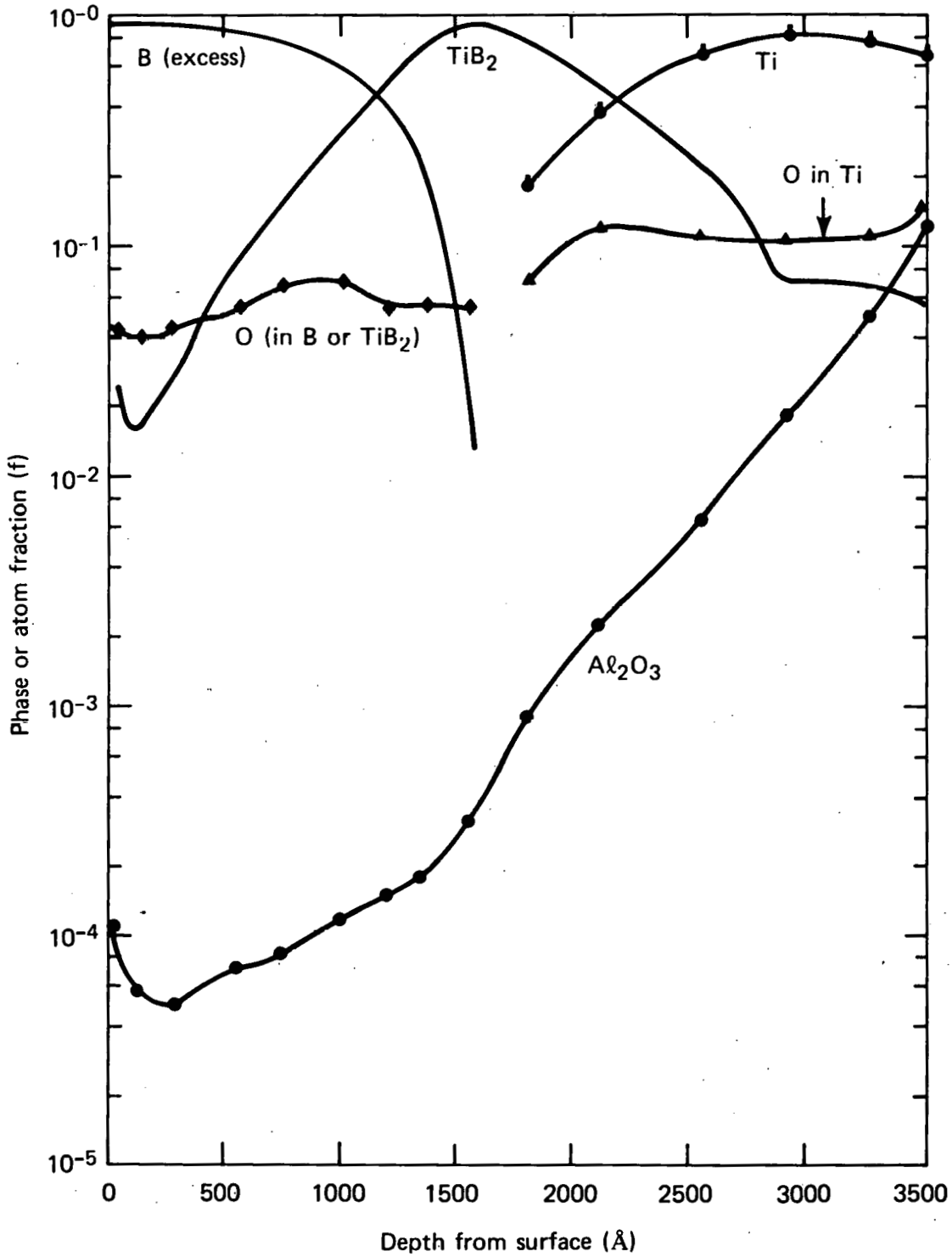

Fig. 8 Concentration-depth profiles from the sputtering of sample $TiB_2$285C (B/Ti/sapphire heated in a He atmosphere for 7.8 min. at 850°C).

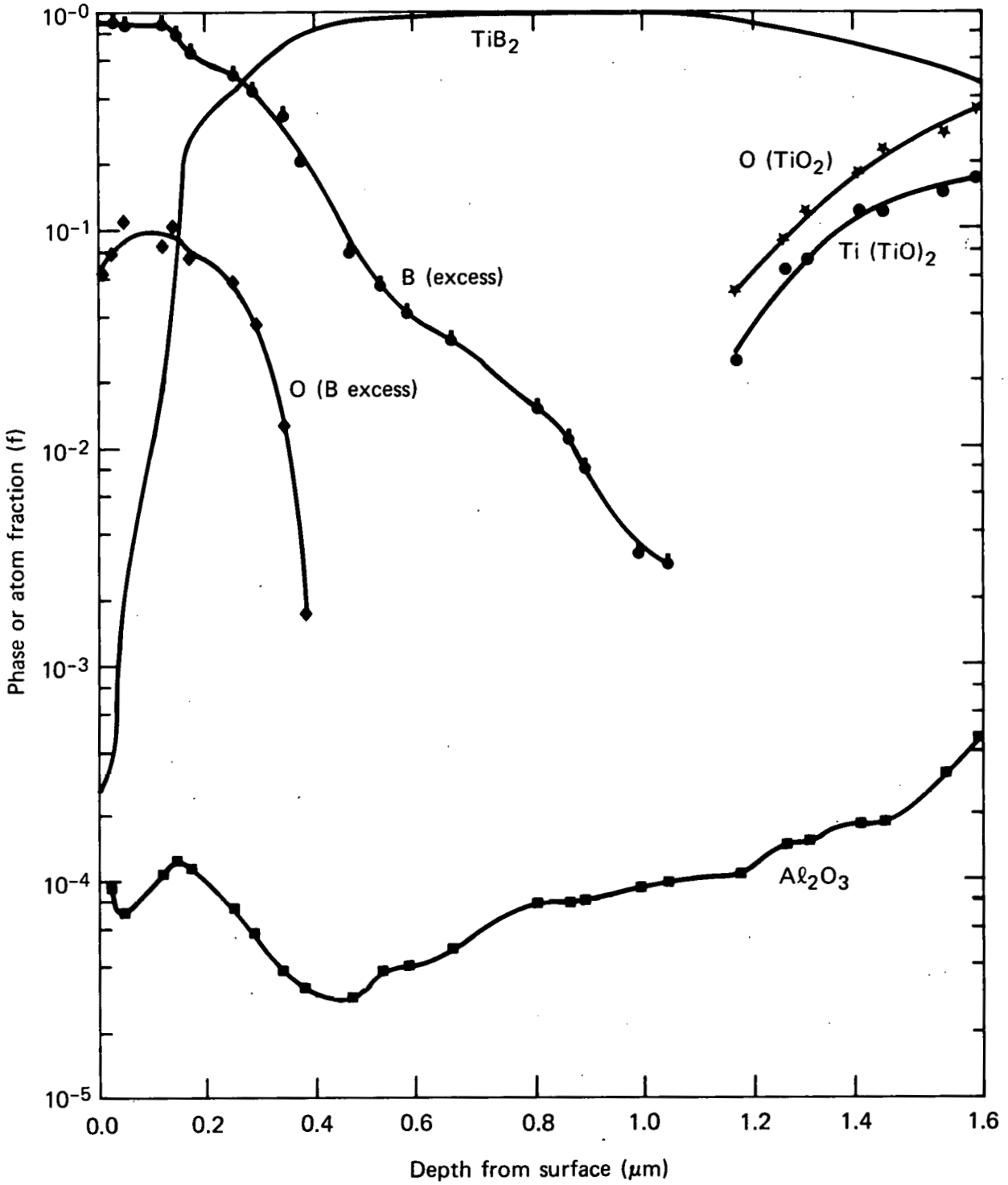

Fig. 9 Concentration-depth profiles from the sputtering of sample $TiB_2$299B (B/Ti/alumina ceramic heated in a He atmosphere for 3 hours at 950°C).

Also presented for comparison are the values from reference (2). The Arrhenius plot, (log k vs 1/T) from Thebault's paper, along with the data obtained in this study is shown in Figure 10. The data points obtained here fall consistently below the previously reported results of Thebault et al. A lower activation energy was thus obtained from our work; viz. 18 vs 25 kcal/mol. No conclusive arguments as yet have been advanced to explain the discrepancies between our results and those quoted. The temperature measurements are accurate to within $\pm$ 5°C. The most serious errors probably arise in the assumptions made concerning the SIMS profile calculations. The thickness measurements have a rather large error band ($\pm$ 10%). Perhaps the agreement is good considering all the difficulties in interpreting the SIMS results. There is also a question of the role of impurities in altering the diffusion characteristics. Thebault has thus observed a lowering of the diffusion constant for B_4C-coated boron fibers and an increase in the activation energy.[2] The film sources in this work are, however, of high purity, making the impurity argument unlikely.

An additional observation which should be mentioned is the possibility of a competitive reaction between titanium and the substrate. At lower temperatures and shorter reaction times this is less of a potential problem and may be consistent with the closer agreement of the low temperature diffusion constant. At the higher temperature (and with thicker film couples), a competitive reaction is more likely to occur. Support for this is further seen in examining the Ti - substrate region for film $TiB_2$299B (Figure 9). At the substrate the Ti and O profiles run parallel, suggesting that some of the Ti has reacted to form either TiO_x or $Ti\ Al_y O_z$. This could then result in a smaller predicted TiB_2 thickness (or a larger k). The same argument can rationalize the 850°C result, except for the reaction time.

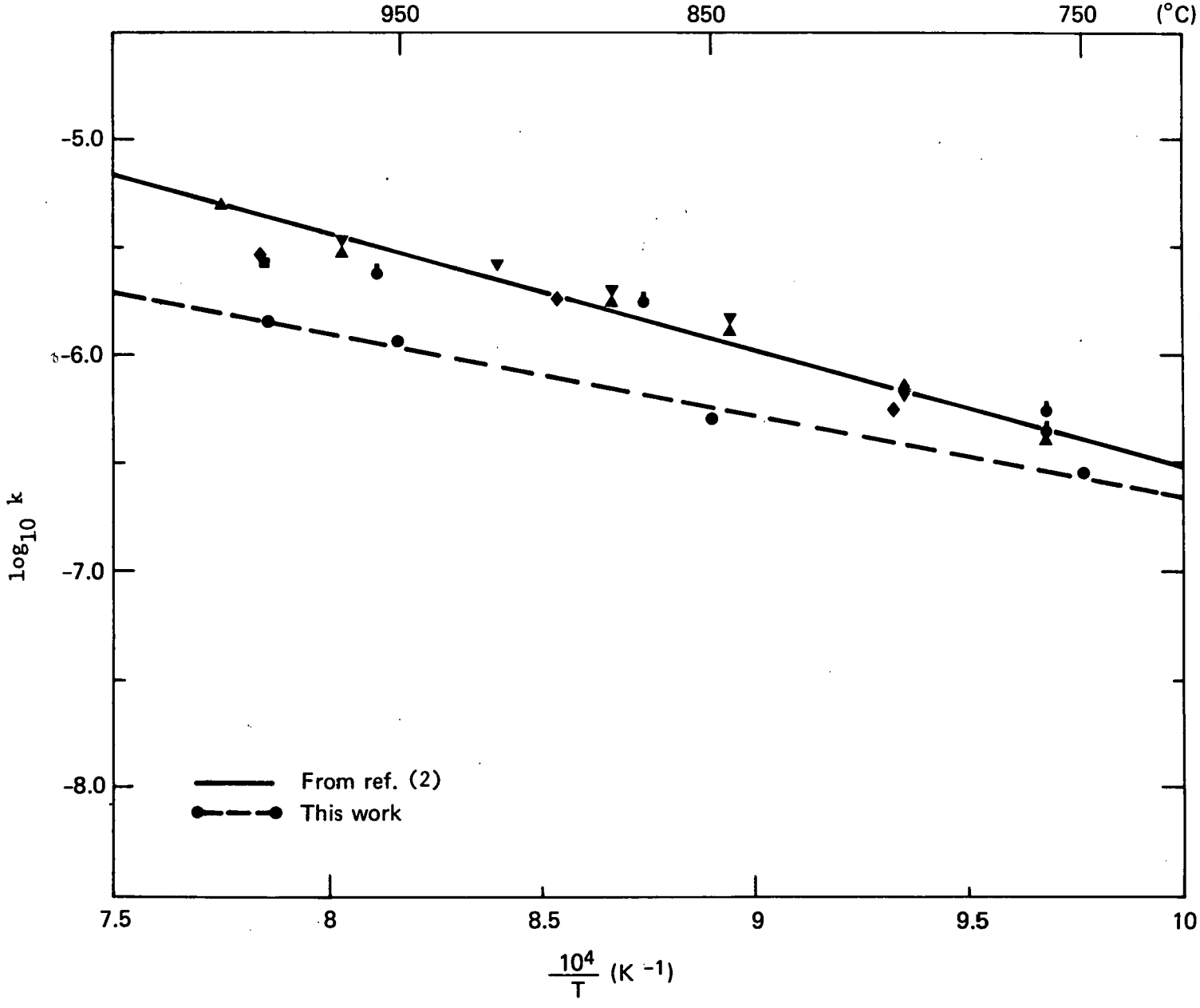

Fig. 10 Arrhenius plot of TiB_2 reaction rate constant vs inverse temperature. Data from this work and from Thebault et al. are shown.

The low value of the reaction constant is surprising since it is generally assumed that freshly deposited polycrystalline films would be more reactive than the bulk material. The heating times used in forming TiB_2, as listed in Table V, were determined assuming the bulk reaction rates. For samples $TiB_2$276, $TiB_2$291, and $TiB_2$299, the reaction times at 950°C were, however, not sufficiently long according to the newly determined rate constant. Thus, from Eq. (3), with $k = 11.7 \times 10^{-7} cm/sec^{\frac{1}{2}}$, sample $TiB_2$299B should have been heated for about 7.3 hours rather than for 3 hours. The reaction of the under-heated samples would, of course, be completed during the outgassing stage of the silicon deposition.

4. PHOTOVOLTAIC DEVICES

4.1 Photovoltaic Device Fabrication

Samples Si 238D, Si*240E, and Si*240B were processed into complete devices. The silicon film parameters for the Si 238 series were given in the last quarterly report.[1] The parameters for the Si*240 series are given in Table I of this report. The junctions in all three samples were formed by the n-diffusion process described in prior reports. Sample Si*240E (as well as Si 238D) was processed at 975°C, which is similar to that used in most previous samples, and Si*240B was processed at 900°C. It was felt that the lower temperature might improve the device characteristics. The schedule for processing the samples is presented in Table VII.

TABLE VII

THIN FILM SILICON PHOTOVOLTAIC DEVICE PROCESSING STEPS.

	PROCESS/SAMPLE	Si*240E	Si*240B
1	CLEAN	Boil Acetone	Boil Acetone
2	ETCH	BOE 10 min → 30 min H_2O	BOE 10 min → 30 min H_2O
3	OXIDATION	4 hrs. @ 975°C	10 hrs @ 900°C
4	PHOTOLITHOGRAPHY	Level 1 Mask	Level 1 Mask
5	PRE-DIFFUSION ETCH	2.5% HF, 10 sec → 20 min H_2O	2.5% HF 10 sec → 20 min H_2O
6	DIFFUSION - n-Type Flow Rates: N_2 O_2 PH_3	6.5 min. @ 975°C 3300 ml/min 44 ml/min 16.5 ml/min	12 min. @ 900°C 2870 ml/min 44 ml/min 165 ml/min
7	POST-DIFFUSION ETCH	2.5% HF 45 sec → 20 min H_2O	2.5% HF 45 sec → 20 min H_2O
8	OXIDATION	1 hr. @ 975°C	2 hrs @ 900°C
9	PHOTOLITHOGRAPHY	Level 2 Mask	Level 2 Mask
10	PRE-ELECTRODE ETCH	2.5% HF 10 sec → 20 min H_2O	2.5% HF, 10 sec → 20 min H_2O
11	ELECTRODE DEPOSITION	Through Mask	Through Mask

The processing schedule at 900°C was selected to achieve the same junction depth as the 975°C processing, thus different times for diffusion as well as different flow rates were required for the drive-in oxidation. These times were estimated from the diffusion constants determined previously. Following the oxidation (Step 8 in Table VII) windows are opened up in the oxide in preparation for electrode deposition.

The electrode deposition was carried out this quarter by means of deposition through masks rather than by the photolithographic process used previously. The vacuum electrode deposition masks, as described in the last quarterly report, were formed from two-mil thick stainless-steel and were used for the electroding of Si 238D. These masks were somewhat coarser than necessary; the designed openings were too big and the fingers rather far apart. Consequently, a new set of masks was fabricated and used in the electrode deposition of samples Si*240B and Si*240E. Sample Si 237D was also etched and re-electroded with the new pattern. The mask pattern designated F-1 is formed of 1 mil thick kovar and shown in Figure 11. The design dimensions of the mask are given in Table VIII.

TABLE VIII

DESIGN DIMENSIONS OF DEVICE PATTERNS (F-1)

DEVICE PATTERN	n-DIFFUSION WINDOW AREA (cm^2)	ELECTRODE AREA (cm^2)	"EFFECTIVE" ACTIVE AREA (cm^2)	ACTIVE AREA (%)
A	1.00645	0.12935	0.87710	87.1
B	0.18387	0.02694	0.15693	85.3
D1, D5	2.32258×10^{-2}	0.35484×10^{-2}	1.96774×10^{-2}	84.7
D2, D3	5.80644×10^{-3}	1.12903×10^{-3}	4.67741×10^{-3}	80.6
C4, D4	2.58064×10^{-3}	0.64516×10^{-3}	1.93548×10^{-3}	75.0
C1, C2, C3	1.45161×10^{-3}	0.16129×10^{-3}	1.29032×10^{-3}	88.9
Bottom Electrode	N/A	4.83870×10^{-2} (Deposited Area)	3.61290×10^{-2} (Oxide Window Area)	N/A

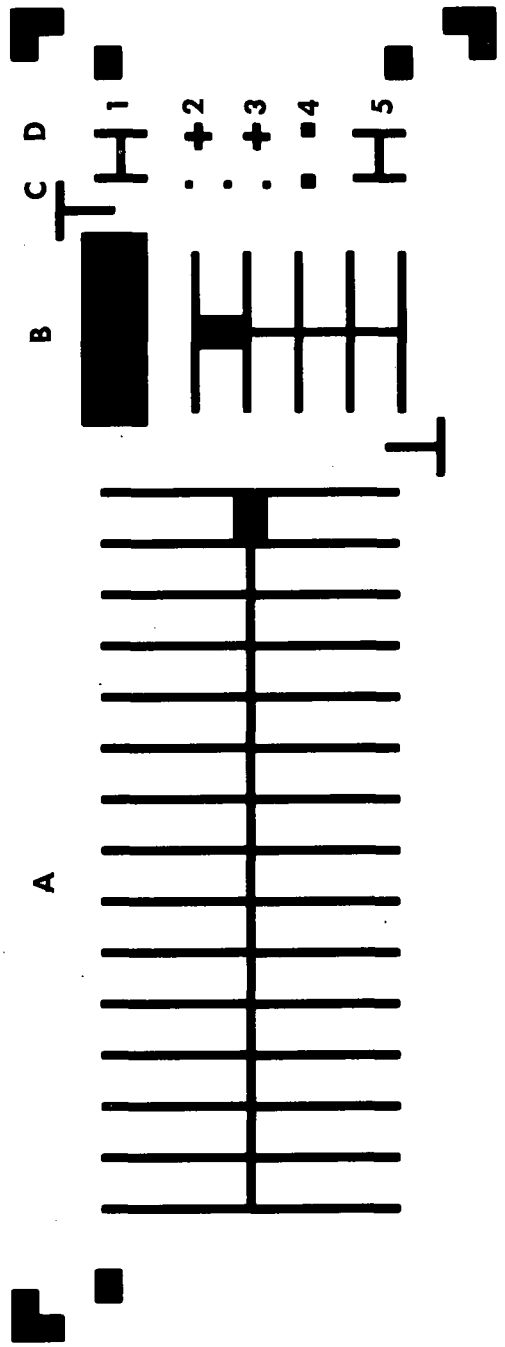

Fig. 11 Electrode deposition mask, Pattern F-1

The original intent was to make heavy masks which could support the six substrates fabricated in each run. Since six samples were not being processed at one time and since alignment of the masks with the photolithographically defined n-type regions was likely to prove difficult, the simple expediency of aligning each individual substrate by hand proved to be more feasable. There appeared to be little loss in definition between the mask and the evaporated pattern on the substrate. There was, however, a significant definition deterioration between the photolithographically designed pattern and the actual etched masks. These differences are indicated in Table IX for devices using both F-1 and F masks.

TABLE IX

MASK DEPOSITED ELECTRODE AREAS

PATTERN	DESIGN AREA cm^2	MASK AREA cm^2	FILM AREA cm^2
F, (2 mil thick) D2	6.5×10^{-4}	9.2×10^{-4}	9.2×10^{-4}
F-1, (1 mil thick) D-1	3.5×10^{-3}	5.7×10^{-3}	5.8×10^{-3}
C-1	1.6×10^{-4}	3.0×10^{-4}	3.5×10^{-4}

The masks used were clearly overetched. More careful etching procedures would have resulted in the areas conforming more closely to the design. A photograph of a portion of the electrode deposition masks and the resulting pattern on Si 237B is shown in Figure 12. (Si 237B was re-electroded in order to test the new masks.) No sintering was carried out following the electrode deposition.

In addition to the electrode mask, sets of "n-type" diffusion masks for photolithography and a matching n-type deposition mask for use in the vacuum system were fabricated. The deposition mask was

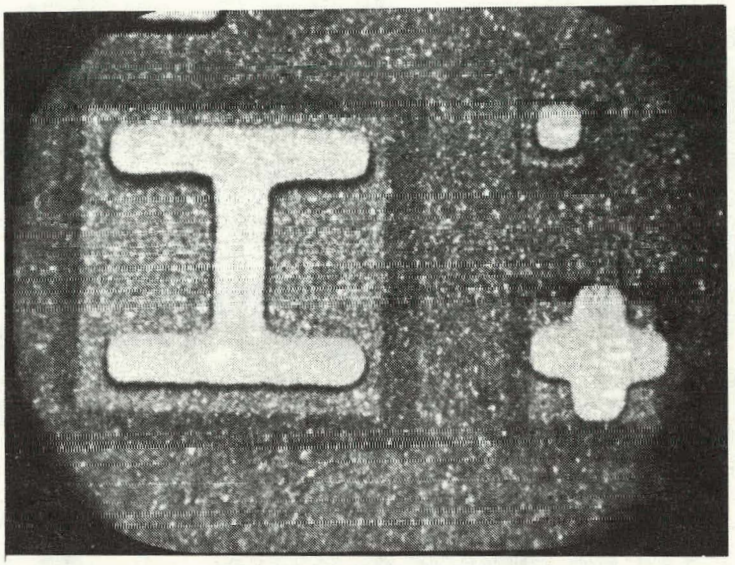

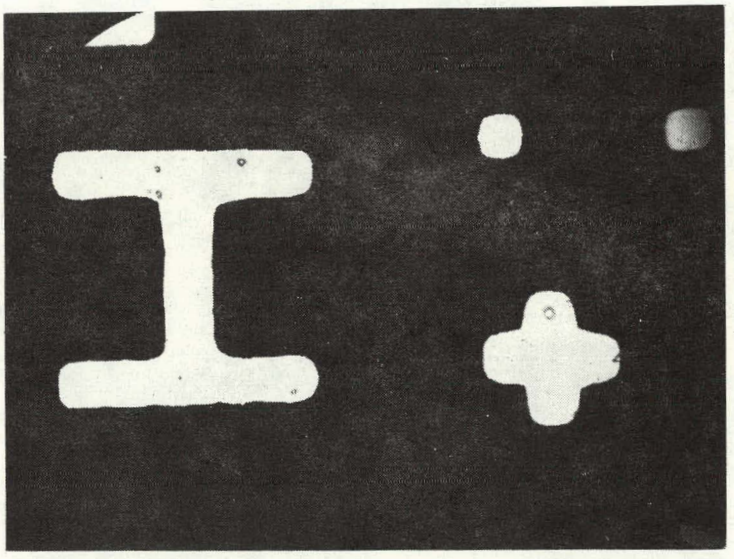

Fig. 12 a. Region of 1 mil overetched electrode mask. (∿ 31X)

b. Corresponding deposited Ti/Ag film through the mask.

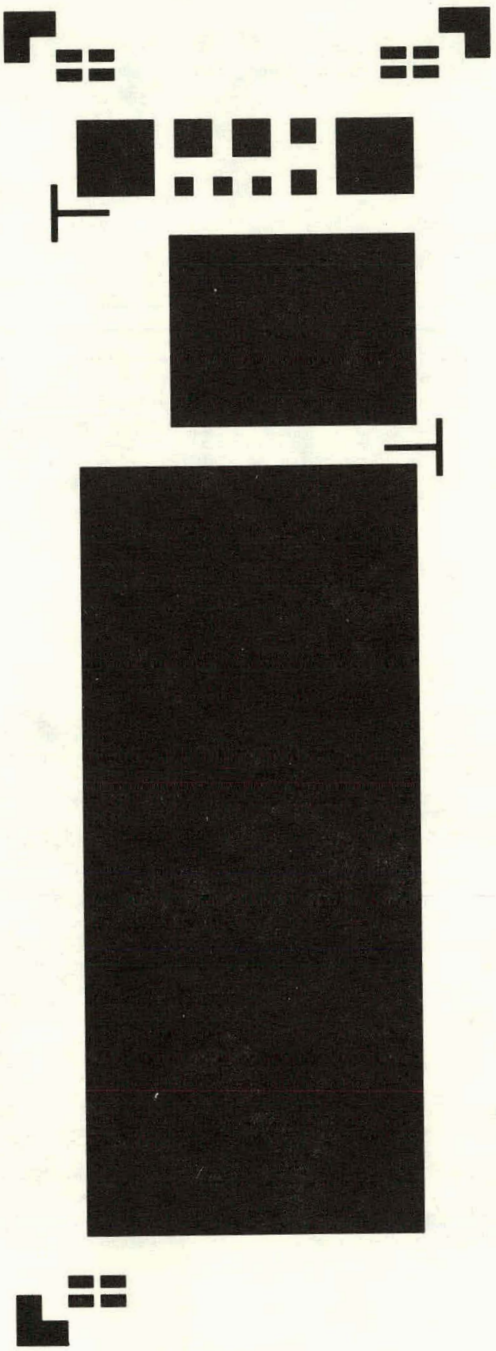

Fig. 13 Diffusion pattern for photolithography, Pattern F1.

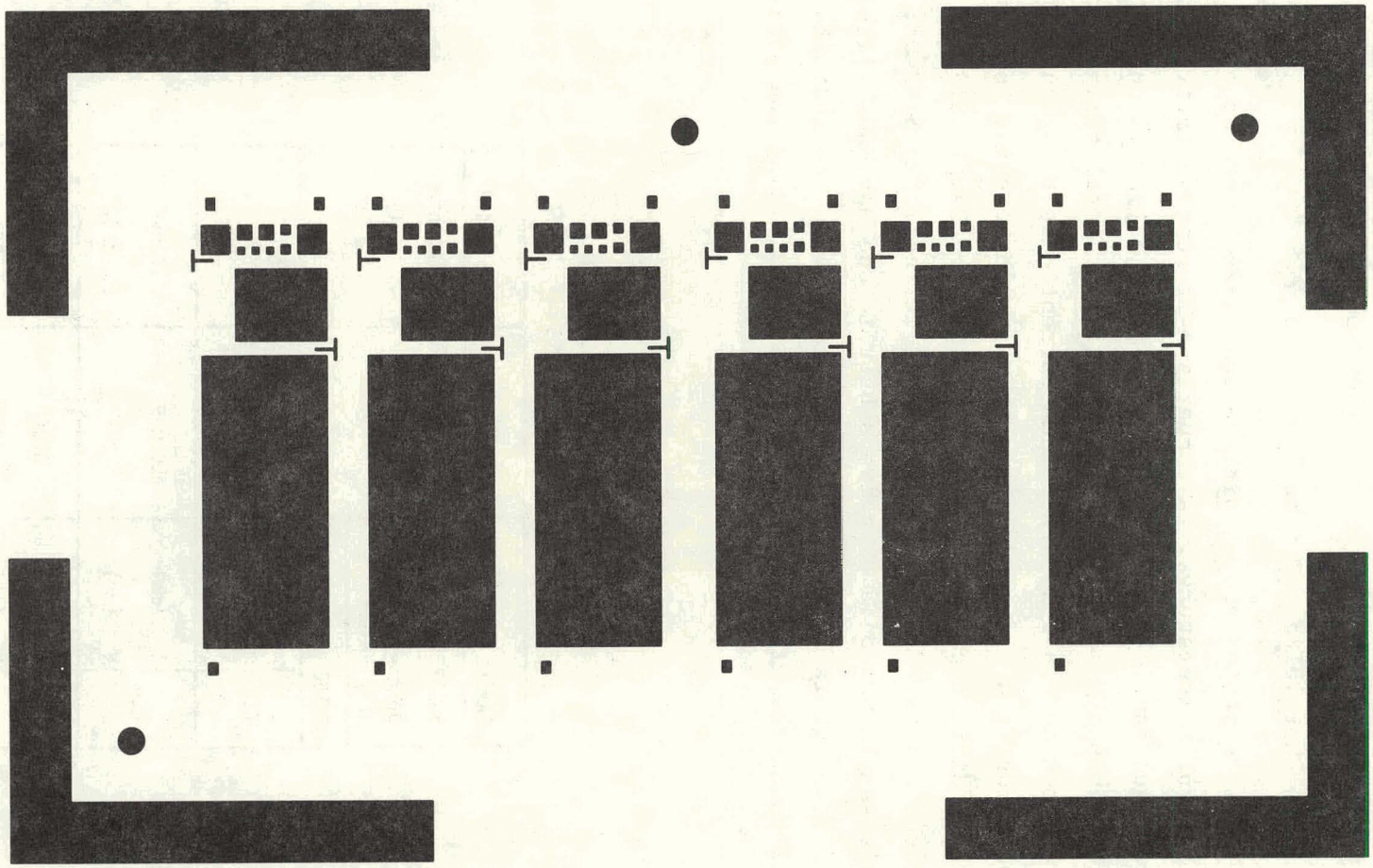

Fig. 14 Evaporation mask for n-region (six samples), Pattern F-1

formed of 5 mil tantalum and fits into the standard 6-position tantalum substrate holder. Figure 13 illustrates the photolithographic pattern and Figure 14, the deposition masks.

4.2 Photovoltaic Device Properties

As stated above, Si*240B and Si*240E were processed at different temperatures. A comparison of representative devices from each sample is listed in Table X and a typical current-voltage oscilloscope trace is shown in Figure 15. Total currents are presented in Table X rather than current density because of the poorly defined electrode patterns. As can be seen, there is little difference between the two samples. Sample Si*240B may have a slightly higher short circuit-current than Si*240E; however, this sample was on a sapphire substrate and may have slightly different grain structure. These results tend to indicate that the diffusion temperature is not the feature limiting the efficiency of the cells.

TABLE X

COMPARISON OF DEVICES PROCESSED AT DIFFERENT TEMPERATURES

SAMPLE		Si*240E	Si*240B
SUBSTRATE		Alumina	Sapphire
PROCESSING A TEMPERATURE		900°C	950°C
DEVICE			
C2	I_{sc} (ma)	0.010	0.014
	V_{oc} (mV)	292	286
D-2	I_{sc} (ma)	0.035	0.046
	V_{oc} (mV)	248	243
D-3	I_{sc} (ma)	0.046	0.060
	V_{oc} (mV)	209	291

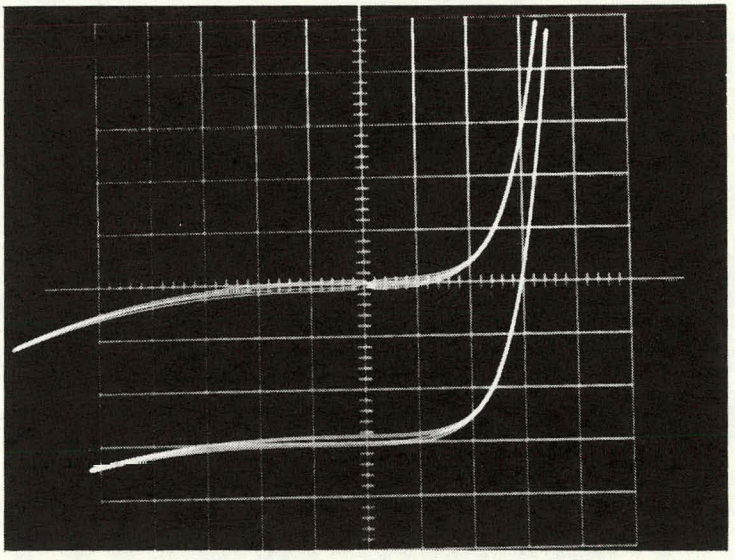

Fig. 14 Evaporation mask for n-region (six samples), Pattern F-1

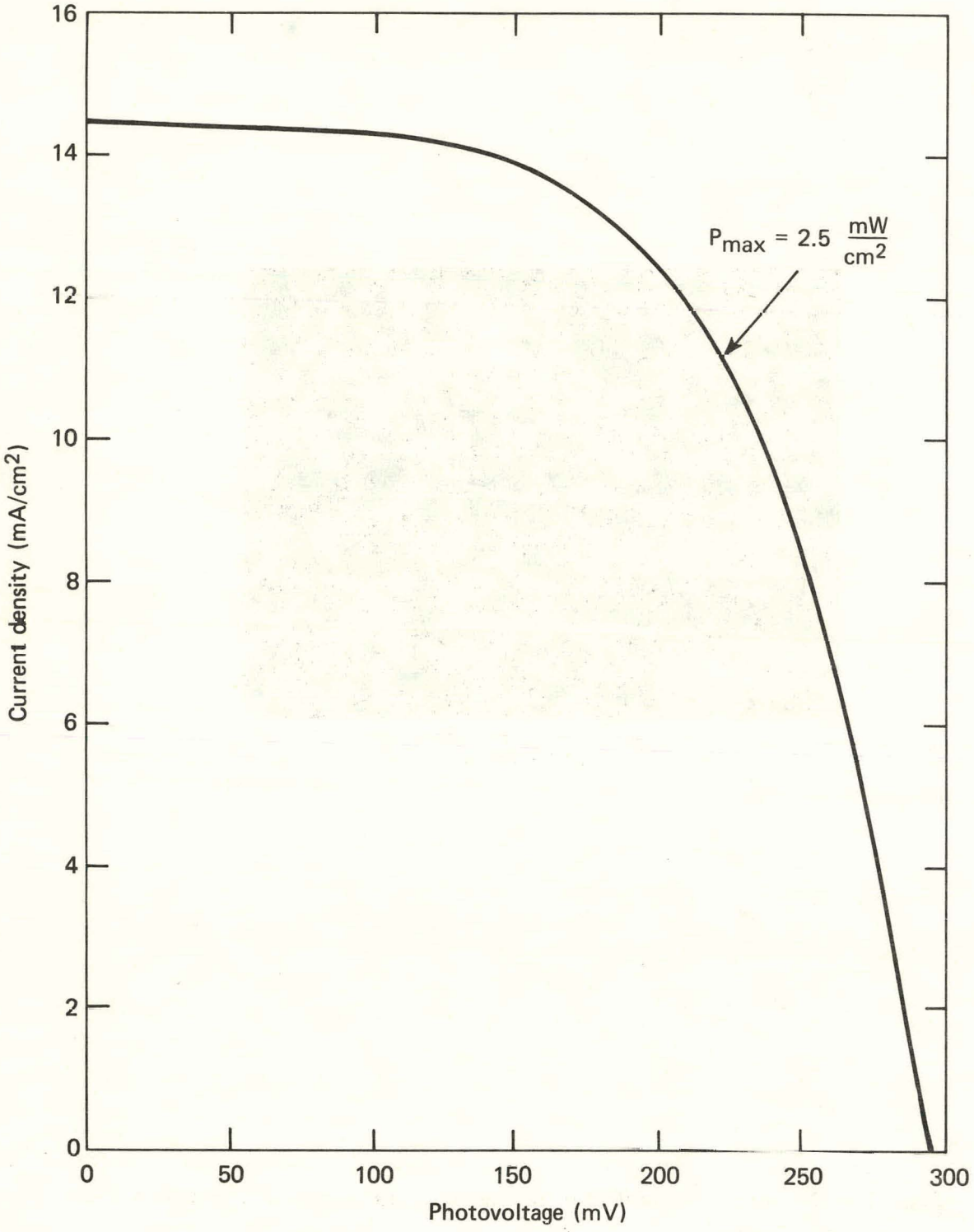

Fig. 16 Photovoltaic response to AM-1 simulated insolation (100 mW/cm^2), sample Si 238D (Device D2).

Sample Si 238D was processed in a way similar to the schedule in Table VII for Si*240E. The photovoltaic characteristic is shown in Figure 16 for AM-1 (100 mW/cm^2) simulated insolation. Important parameters are: η = 2.50%, V_{oc} = 296 mV, J_{sc} = 14.5 mA/cm^2, ff = 0.58, A_{eff} = 4.6 X 10^{-3} cm^3. The quantum efficiency is plotted in Figure 17. This is nearly identical with the quantum efficiency curves reported earlier. Using the method described in the First Quarterly Report, the minority carrier diffusion length L_D = 3.1 μm. The average surface grain size for this sample was approximately 12 μm. Thus, the conclusion drawn last quarter still holds: that grain size may not be limiting the diffusion length.

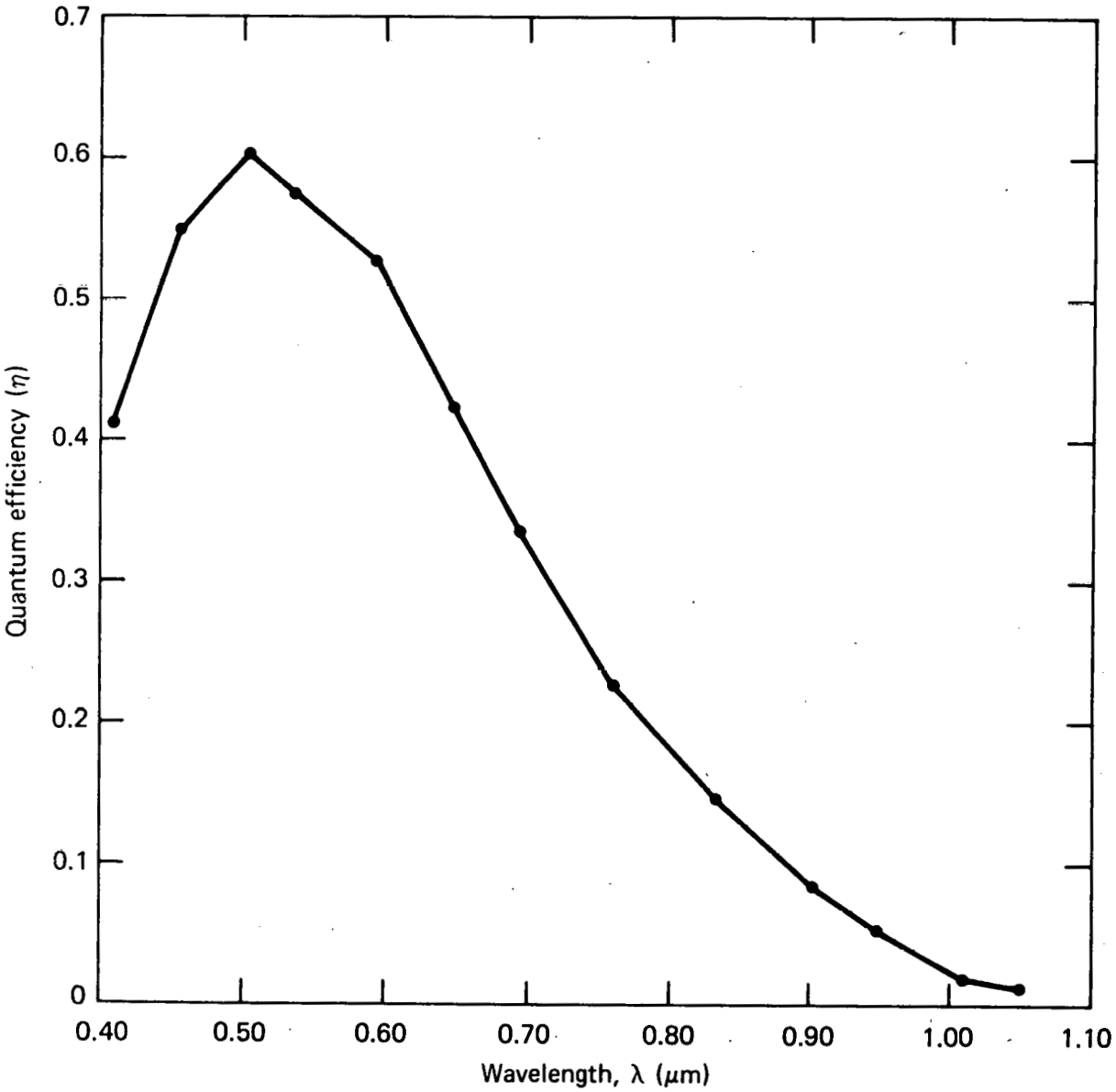

Fig. 17 Spectral quantum efficiency, sample Si 238D (D2).

5. DISCUSSION AND PLANS FOR NEXT QUARTER

Progress has been made this quarter towards the goal of an "all-vacuum deposited" solar cell. Deposition of n-doped silicon was carried out in the oil-diffusion-pumped system and the top electrodes were deposited through a mask pattern rather than by the photolithographic process. The titanium and boron depositions were carried out in a single chamber without breaking the vacuum, thus simplifying the process of forming the bottom electrodes.

The change in the procedures for forming the top electrode, from the wet etching process required for photolithography to the vacuum deposition process, has not altered the photo-response of the samples. There was some concern that the etching process and subsequent rinsing could leave residual metal ions in the grain boundaries which were not removed by the careful cleaning procedures and that these metal ions might have a detrimental effect on the photovoltaic response.

The source of impurities, chiefly related to molybdenum, in the ion-pumped system was removed and the purity of the samples produced in that system is now equal to or better than those produced in the oil-diffusion-pumped system. Pressure during deposition is about two orders of magnitude lower in the ion-pumped system than in the oil-pumped chamber. It is anticipated that photovoltaic devices made from these purer films will be made and completed during the coming quarter.

The reaction constants and the activation energy required to form the TiB_2 layers was determined and found to be less than those reported by other authors for bulk material. According to the newly determined reaction constants some of the samples were not heated sufficiently to obtain complete reaction prior to the resistivity determinations. Reaction was, of course, completed in the silicon deposition system. Some of the variation in measured resistivity may be due to this insufficient heating. This

will be determined next quarter. In addition, there is a time required for removal of the excess boron. Plans are to study the boron loss more thoroughly next quarter. The long heating step required to assure TiB_2 stochiometry does not essentially interfere with the overall process because the complete heating cycle could be carried out in the silicon system during the outgassing stage without any loss of time.

The exact conditions for achieving the best silicon crystallite growth on the bottom electrode have not yet been determined. While the conditions for epitaxial growth (e.g., Si*243B) have been achieved on uncoated sapphire and silicon, the requirement for the bottom electrode coating necessitates an understanding of the silicon-TiB_2 reaction. It may be that the temperatures and deposition rates necessary for the formation of the reacted Si-Ti-B layer ($TiSi_2$) is different from that required for the deposition of the subsequent pure silicon layer. Work on this aspect of the problem is continuing.

The photovoltaic devices formed this quarter served to test the use of the deposition masks for the top electrode. No improvement in device efficiency above the 2 to 3% expected was obtained during this period. However, it is anticipated that the changes outlined above and better purity will lead to improved devices during the coming quarter.

6. REFERENCES

(1) C. Feldman et al., "Vacuum Deposited Polycrystalline Silicon Films for Solar Cell Applications," Quarterly Report, Sept. 15, 1979 to Dec. 31, 1979, work performed under SERI Subcontract XS-9-8278-1, Report No. SERI/XS9/82781-1, The Johns Hopkins University, Applied Physics Laboratory, March 1980.

Also, C. Feldman et al., Final Report, DOE/ET-32208-4, Dec. 1979.

(2) J. Thebault, R. Pailler, G. Bontemps-Moley, M. Bourdeau, and R. Naslain, "Chemical Compatibility in Boron Fibre - Titanium Composite Materials," J. of the Less Common Metals, 47, 221 (1976).

U.S.GOVERNMENT PRINTING OFFICE:1980 740-145/483